# A Fast Level Set Based on New Signed Pressure Force Function for Nuclei Images Segmentation

Ru Xu[1,*], Wei Zhang[2], Guangfang Yang[3]
[1,*]*College of Big Data and Intelligent Engineering, Yangtze Normal University, Chongqing 408100, China*
[2]*College of Computer Science, Chongqing University, Chongqing 400030, China*
[3]*College of Mathematics and Statistics, Chongqing University, Chongqing 400044, China*

Keywords: Image Processing, Level set method, Signed pressure force, Legendre polynomials, Edge stopping function.

Abstract: In the paper, a fast level set for nuclei images is proposed. It is performed with a novel method, mainly combining idea of signed pressure force function with Legendre polynomials. The advantages of the proposed method are as follows. On the one hand, a controlled signed pressure force function based on 1-D Legendre polynomials ($LPSPF^{+}$) can stop the final contours at blurred and multiple objects edges, especially for nuclei images segmentation. On the other hand, we set multiple ball contour as initial contour to automatically detect the exterior and interior boundaries in the image. Ultimately, an improved edge stopping function is applied to fast and robustly capture the edge of multiple regions of interest (ROI). Experimental results demonstrate that our method is higher and faster accuracy than other models on nuclei images and other images with large size, or low-contrast.



## 1 INTRODUCTION

Image segmentation is an essential problem, which is applied to divide the given image into several sections, including ROI and background, especially for the clinical diagnosis from medical images. To execute nuclei images segmentation well, a variety of research has been done and many excellent methods have been presented, like watershed-based segmentation and active contour models (ACM). However, the former has limitation that is prone to over-segmentation. To catch final ROI, the basic thought of ACM is to evolve a curve for the detected target according to energy-minimizing theory.

The established ACM can be widely classified into two categories: region-based models and edge-based models. Besides, some models which combine edge-based models with region-based models have been presented in recent years. And edge-based models mainly rely on the gradient image to stop the evolution of variation curve. Nevertheless, region-based models almost employ statistical characteristic inside and outside the active contour to restrict the evolution of curves.

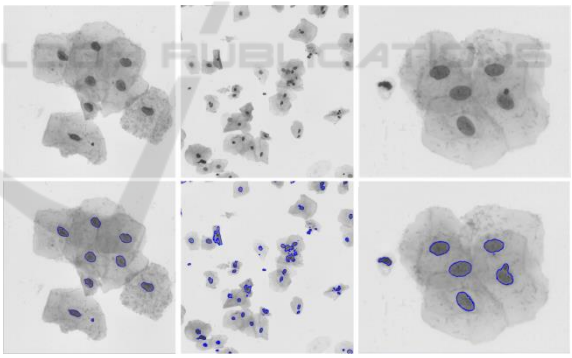

Figure 1: Segmentation results of our method on polynuc -lear images. (Blue curves are the final evolving curves.)

In recent years, many high efficient and accuracy solutions have been proposed to amend the weakness of Chan-Vese model (Chan, T. F., 2001). Li *et al.* (Li Chunming, 2008) proposed the LBF model that can accurately extract the local images, but its calculations take a long time. Li *et al.* (Li Chunming, 2010) presented the idea of the Bias field, and it can deal with intensity inhomogeneity problem by calculating and correcting the bias field. Zhang *et al.* (Zhang Kaihua, 2010) proposed a region-based



Xu, R., Zhang, W. and Yang, G.
A Fast Level Set Based on New Signed Pressure Force Function for Nuclei Images Segmentation.
DOI: 10.5220/0008096000100017
In *Proceedings of the International Conference on Advances in Computer Technology, Information Science and Communications (CTISC 2019)*, pages 10-17
ISBN: 978-989-758-357-5

ACM which is performed with a novel level set method, described as SBGFRLS method. And it can reduce the costly re-initialization of the previous level set method to make it more efficient. Based on the idea of SBGFRLS method, various approaches about improved signed pressure force function were proposed successively. An edge independent segmentation approach Legendre Level Set (L2S) which is robust to variations in intensity levels was proposed (Suvadip Mukherjee, 2014). Zhang *et al.* proposed an improved ACM which is driven by the region-scalable and local Gaussian-distribution fitting energy for image segmentation, named the RSLGD model (Zhang Wei, 2017). He *et al.* proposed a promotional local or global ACM that is driven by Legendre polynomials to optimize SBGFRLS method (He Guanghui, 2018). And Hai *et al.* (Min H, 2018) proposed a unique level set method that is a nonlinear approximation method to solve the nonconvex optimization problem, named Local Approximation of Taylor Expansion (LATE) .

The purpose of the paper is to segment nuclei images (Wu Z, 2012, Park C, 2013) in Figure 1, which have several characteristics including multiple objects, large size, low-contrast and some small regions of interest. To tackle these problems, a controllable level set method driven by pressure force function based on 1-D Legendre polynomial is proposed. Meanwhile, we introduce an edge stopping function (ESF) to fast get edge information of nuclei images. Experiments show that our model can enhance efficiency, accuracy and generalization performance of final segmentation results.

The remainder of this paper is planned as follows. Section 2 briefly reviews of the SBGFRLS and L2S method. Section 3 demonstrates the proposed model. In addition, we perform various experiments, make a comparison and explore the quantitative analysis with other models in the Section 4. Eventually, in Section 5, we give a summary for the above work.

# 2 THE RELATED WORK

## 2.1 The SBGFRLS Method

On the base of GAC model and CV model, K. Zhang *et al.* presented selective binary and Gaussian filtering regularized level set (SBGFRLS), which developed a region based on the singed pressure force function (SPF) to effectively stop the contour at weak or blurred edges. This SPF function can control the evolutionary direction. Besides, the opposite symbols around the edges of ROI in the function can make the contour to shrink when it is outside the boundary and to expand when it is inside the boundary. And the SPF function is defined as follows:

$$spf(I(x)) = \frac{I(x) - \frac{c_1 + c_2}{2}}{max\left(\left|I(x) - \frac{c_1 + c_2}{2}\right|\right)} \quad (1)$$

Where the range of $spf(I(x))$ values is $[-1, 1]$ , and $c_1, c_2$ are to mainly approximate two dynamic image average intensity in the regions inside and outside the active contour $C$ (i.e. the zero level set function $\phi$ ). Then $c_1, c_2$ are expressed as equation (2).

$$c_1 = \frac{\int_\Omega I(x)H(\phi)dx}{\int_\Omega H(\phi)dx}, c_2 = \frac{\int_\Omega I(x)(1 - H(\phi))dx}{\int_\Omega (1 - H(\phi))dx} \quad (2)$$

Thus, the gradient descent flow equation of SBGFRLS model can be donated as follows:

$$\frac{\partial \phi}{\partial t} = spf(I(x)) \cdot (div(\frac{\nabla \phi}{|\nabla \phi|}) + \alpha)|\nabla \phi| + \nabla spf(I(x)) \cdot \nabla \phi \quad (3)$$

Where $\alpha$ is a adjustable parameter that can be changed with regard to different images. Moreover, the regular term $div(\nabla\phi/|\nabla\phi|) \cdot |\nabla\phi|$ can be abandoned, because we can use Gaussian filter to smooth the level set function to keep the evolutionary contours regular. Besides, the term $\nabla spf(I(x)) \cdot \nabla\phi$ can be removed because the method utilizes the statistical in formation of the regions. Thus the final gradient descent flow equation is given as in equation (4).

$$\frac{\partial \phi}{\partial t} = \alpha \cdot spf(I(x)) \cdot |\nabla \phi| \quad (4)$$

Experiments show it can distinctly reduce costly computing of previous methods. But the method has a drawback which can't segment images with intensi -ty inhomogeneity.

## 2.2 The L2S Method

In 2014, Suvadip *et al.* presented a novel region-based segmentation method by employing Legendre polynomials to approximate image region intensity, and it can effectively solve the image with intensity inhomogeneity problem. The significant contribution of the L2S method is to formalized and generalize the classical CV model, which can replaced the two scalars $c_1, c_2$ with two continuous derivable functions

$c_1^n(x), c_2^n(x)$ defined in equation (5). And the two fun -ctions are assumed to be a linear combination of a few Legendre basis functions, respectively.

$$c_1^n(x) = \sum_k \alpha_k L_k(x),\ c_2^n(x) = \sum_k \beta_k L_k(x) \quad (5)$$

Where $L_k$ is a multidimensional Legendre polynomi -al. Its meaning is the outer product of the 1-D counterparts which can be written easily. However, we can get the 2-D Legendre polynomial by computing $L_k(x,y) = l_k(x)l_k(y),\ (x,y) \in \Omega \subset [-1,1]^2$. Then $l_k$ is a simple 1-D Legendre polynomial which can be written as:

$$l_k(x) = \frac{1}{2^k}\sum_{i=0}^{k}\binom{k}{i}(x-1)^{k-i}(x+1)^i \quad (6)$$

Therefore, we can write the energy functional of the L2S model as the following formula:

$$\begin{aligned} E^{L2S}(\phi) = &\int_\Omega \left|I(x) - L(x)A^T\right|^2 H(\phi(x))dx + \lambda_1\|A\|_2^2 \\ &+ \int_\Omega \left|I(x) - L(x)B^T\right|^2 (1-H(\phi(x)))dx + \lambda_2\|B\|_2^2 \\ &+ \mu\int_\Omega \delta(\phi(x))\frac{\nabla\phi(x)}{|\nabla\phi(x)|}dx \end{aligned} \quad (7)$$

Where $\lambda_1 \geq 0, \lambda_2 \geq 0, \mu \geq 0$ are three adjustable para -meters. And the regularized Heaviside function $H(\phi)$ can be defined as equation (8). The derivative of $H(\phi)$ is on behalf of the dispersed Dirac function expressed as follows.

$$H_\varepsilon(x) = \frac{1}{2}(1 + \frac{2}{\pi}\arctan(\frac{x}{\varepsilon})) \quad (8)$$

$$\delta_\varepsilon(x) = \frac{\varepsilon}{\pi(\varepsilon^2 + x^2)} \quad (9)$$

In order to compute optimal $A$ and $B$, we can perform $\partial E/\partial A = 0$ and $\partial E/\partial B = 0$, then the symbolic solution $\hat{A}$ and $\hat{B}$ can be caught by computing the equation (10) and (11).

$$\hat{A} = [P + \lambda_1 \cdot M]^{-1}\int_\Omega L(x)I(x)H(\phi(x))dx \quad (10)$$

$$\hat{B} = [Q + \lambda_2 \cdot M]^{-1}\int_\Omega L(x)I(x)(1-H(\phi))dx \quad (11)$$

Where $M, P$ and $Q$ are defined in (Suvadip Mukherjee, 2014), and discretization of expression are written as:

$$[P]_{i,j} = H(\phi(x)) < d_i, d_j > \quad (12)$$

$$[Q]_{i,j} = (1 - H(\phi(x))) < d_i, d_j > \quad (13)$$

Where $<,>$ indicates the Euclidean inner product operator and $0 \leq i, j \leq N$. Then, the following gradient descent flow equation can be deduced.

$$\begin{aligned} \frac{\partial\phi}{\partial t} = &\delta_\varepsilon(\phi)\left(-\left|I(x) - L(x)\hat{A}^T\right|^2 + \left|I(x) - L(x)\hat{B}^T\right|^2\right) \\ &+ \mu\cdot\delta_\varepsilon(\phi)\cdot div(\frac{\nabla\phi}{|\nabla\phi|}) \end{aligned} \quad (14)$$

Note that the initial boundary value conditions are expressed as the following equation.

$$\phi|_{t=0} = \phi_0\ ,\ \frac{\delta_\varepsilon(\phi)}{|\nabla\phi|}\frac{\partial\phi}{\partial\hat{n}} = 0 \quad (15)$$

Ultimately, it commendably segments images with intensity inhomogeneity. However, the CPU time of results take a long time because of Legendre basis functions. And it can't deal with images including multiple objects, like nuclei images.

## 3 THE PROPOSED METHOD

Like existing level set methods, we still hypothetical -ly reflect on a image, like nuclei images. For each pixel $x$ in the given image, let $\phi^0 = \{x : \phi(x) = 0\}$ is the zero level set function that partitions image $I$ into two parts $\Omega_1 = \{x : \phi(x) > 0\}$ and $\Omega_2 = \{x : \phi(x) < 0\}$. In fact, we can minimize the entire energy functional of $I$ to get the ideal segmentation results.

First of all, the gradient descent flow equation of L2S model can be reworded as equation (16) by deducing the equation (14) .

$$\begin{aligned} \frac{\partial\phi}{\partial t} = &\delta(\phi)\left(2L(x)(\hat{A}^T - \hat{B}^T)\cdot(I(x) - \frac{L(x)(\hat{A}^T + \hat{B}^T)}{2})\right) \\ &+ \mu\cdot\delta(\phi)div(\frac{\nabla\phi}{|\nabla\phi|}) \end{aligned} \quad (16)$$

Where $A = (a_1, a_2, \cdots, a_N)$ and $B = (b_1, b_2, \cdots, b_N)$ are the coefficient vectors for two regions $\Omega_1$ and $\Omega_2$, while $N = (m+1)^2$ is the number of basis functions and $m$ is the degree of Legendre polynomial (i.e. $m$-D Legend -re polynomial). Note that 0-D Legendre polynomial reduces to the famous CV model, thus

the proposed model presents a generalized framework.

In practice, we often use 1-D Legendre polyno -mials, i.e. $m=1$. Particularly, we assume that the purpose is to segment an image $I$ with $300\times300$ size. By computing and analyzing the parameters, the size of $\hat{A}^T, \hat{B}^T, L(x)$, $L(x)(\hat{A}^T-\hat{B}^T)$ and $L(x)(\hat{A}^T+\hat{B}^T)$ are $4\times1$, $4\times1$, $300^2\times4$, $300^2\times1$ and $300^2\times1$. However, in our experiments, the term $L(x)(\hat{A}^T-\hat{B}^T)$ is resized as $L(x)(\hat{A}^T+\hat{B}^T)$ with $300\times300$ size, according to the original image size.

Inspired by (Zhang kaihua, 2010, Suvadip Mukherjee, 2014, and He Guanghui, 2018), on the one hand, we combine advantage of L2S model with SBGFRLS model to develop a new SPF function based on Legendre polynomial with signed pressure force function (LPSPF$^+$), which can be donated as follows.

$$lpspf^+(I(x))=\frac{I(x)-\frac{L(x)(\hat{A}^T+\eta\cdot\hat{B}^T)}{1+\eta}}{max\left(\left|I(x)-\frac{L(x)(\hat{A}^T+\eta\cdot\hat{B}^T)}{1+\eta}\right|\right)} \quad (17)$$

Where $lpspf^+(I(x))$ combines $spf(I(x))$ with 1-D Legendre polynomial to overcome the problems of SBGFRLS model that is not good for images with intensity inhomogeneity. Different from SBGFRLS model, we add a parameter $\eta$ to effectively restrain convergence scale inside or outside of ROI.

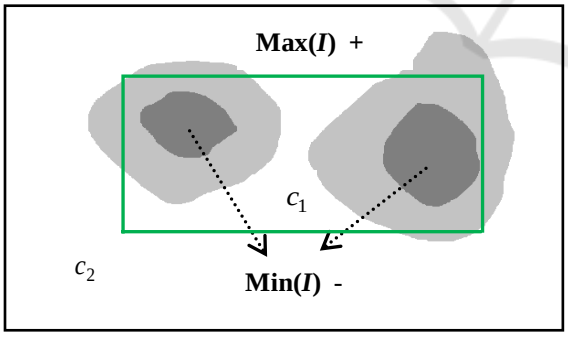


Figure 2: The labels of the SPF function inside and outside the object are opposite.

The significance of $lpspf^+(I(x))$ can be explained as follows. With regard to Figure 2, we assume that the intensities inside and outside the $C$ are homogene -ous. It is intuitive that $Min(I)\le c_1,c_2\le Max(I)$ in the SBGFRLS model. Since we substitute scalars $c_1, c_2$ by two continuous derivable functions $c_1^n(x), c_2^n(x)$, it is similar that $Min(I(x))\le c_1^n(x), c_2^n(x)\le Max(I(x))$, and equal labels cannot be caught synchronous wherever the contour is. So,we can deduce equation (18).

$$Min(I(x))<\frac{L(x)(\hat{A}^T+\hat{B}^T)}{2}<Max(I(x)) \quad (18)$$

Obviously, the signs of the SPF function in equation (1) are identical to what Figure 2 shows, so equation (17) can serve as an SPF function. Meanwhile, we utilize a constant $\alpha$ to replace $2L(x)(\hat{A}^T-\hat{B}^T)$ for simplicity. Substituting the SPF function in equation (16) for the ESF in equation (5), the level set formulation of the proposed model is as follows:

$$\frac{\partial\phi}{\partial t}=\alpha\cdot\delta(\phi)\,lpspf^+(I(x))+\mu\cdot\delta(\phi)div\left(\frac{\nabla\phi}{|\nabla\phi|}\right) \quad (19)$$

On the other hand, to capture the edges of ROI and speed up the segmentation for images with multiple objects, we employ the edge indicator function $g(\nabla I)$ expressed as equation (20):

$$g(|\nabla I|)=min\left\{\frac{1}{1+|\nabla G_\sigma * I|^2}, exp\left(-\frac{|\nabla G_\sigma * I|^2}{\sigma^2}\right)\right\} \quad (20)$$

Where $\nabla$ and $G_\sigma * I$ are the gradient operator and the convolution of image $I$ with Gaussian function $G_\sigma$. The purpose is to converge smaller values at edges.

Finally, to speed up the convergence, we substitute $\delta(\phi)$ with $|\nabla\phi|$. Thus, the gradient flow equation of our model can be donated as:

$$\frac{\partial\phi}{\partial t}=\alpha\cdot|\nabla\phi|\cdot lpspf^+(I(x))+\beta\cdot|\nabla\phi|\cdot div\left(g(\nabla I)\cdot\frac{\nabla\phi}{|\nabla\phi|}\right) \quad (21)$$

Where $\alpha>0, \beta\ge0$ are two adjustable parameters. And the curvature of level-curve $\phi$ is $div(\nabla\phi/|\nabla\phi|)$. $\beta$ is the parameter of the second term in equation (20). And it's significant that initial boundary value conditions are equation (15). The nature of equation (21) is to solve a partial differential equation with a finite difference method.

# 4 EXPERIMENTAL RESULTS

## 4.1 Data Set and Algorithm of The Pro -posed Model

To demonstrate the efficacy of the proposed method, we have performed experiments on 664 images in 2018 Data Science Bowl. The nuclei data set of stage1_train chiefly can be categorized into 4 classes：107 colorized and multicellular images, 89 low contrast and multicellular images, 16 polynucle -ar images and 452 gray multicellular images. Note that it contains the segmented masked image of all nucleus for each image (i.e. ground truth).

In the paper, we have proposed a fast level set based on combining Legendre Polynomial with signed pressure force function (LPSPF$^+$). Its main implementation can be described at Algorithm 1.

Algorithm 1: The implementation of the proposed method

**Input**: a nuclei image $I(x)$
**Initialization**: $\alpha, \beta, \sigma, \eta, \Gamma, \varepsilon, \phi^0, MaxIter, \delta$
**Output**: level set function $\phi(x)$

1. **for** $i$ = 1: $MaxIter$
2. compute $\hat{A}, \hat{B}$, $lpspf^+(I(x))$ and $g(\nabla I(x))$
3. update $\phi^{i+1}$ by solving equation (21)
4. optimize $\phi$ with $\phi * G_\sigma$ to enhance the efficiency
5. **if** $iter = MaxIter$ or $\left| len(\phi^{i+1}) - len(\phi^i) \right| / len(\phi^i) < \Gamma$
6. stop the iteration
7. **else**
8. repeat step 2 - 4
9. **end**
10. **end**

Where $len(\cdot)$ is to catch the length of $\nabla(H(\phi))$ in Algorithm 1. In the paper, we choose the Gaussian filter to optimize level set function $\phi$. To accelerate the evolution, we utilize multiple ball contour to replace $\phi^0$. Its advantage is to catch gray value and gradient about the target objects as much as possible, so that multiple objects in a image can be segmented fast and automatically. Besides, the parameter $\eta$ can restrain the gray value of the object to be segmented. And $\eta$ is proportion to gray value, and the range of $\eta$ is $\eta \geq 0$.

## 4.2 Results of the Proposed Method

In this section, a variety of nuclei images are used to valid the robustness and performance of our model and its experimental results are shown in Figure 1, Figure 3 and Figure 6. Some recent methods referred in L2S, RSLGD, SBGFRLS, and LGLP are tested on synthetic and real images and above data set to demonstrate advantages of the proposed model. And the whole works are performed in Matlab R2014a on a personal computer with Inter Xeon CPU E3-1226 3.30 GHz and 8GB RAM. By default, those parameters are set as $\alpha = 80$, $\beta = 1$, $\sigma = 1$, $\eta = 4$, $\Gamma = 0.001$, $\varepsilon = 2$, $MaxIter = 100$, $\delta = 1$. The initial con -tour is set as multiple balls which are equally distributed with $r = 25$ in the whole image.

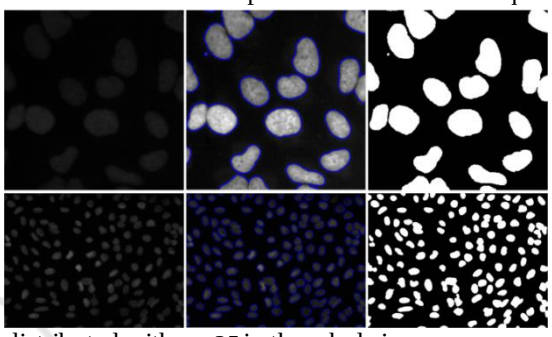

Figure 3: Segmentation results of our proposed method on low-contrast and multicellular images. Col 1: input images. Col 2:segmentation results. Col 3: ground truth. (Blue curves are the final evolving curves.)

On the one hand, according to the segmentation results in Figure 1, Figure 3 and Figure 5, we can observe that the proposed model can accurately get multiple objects boundaries, especially with regard to multicellular or polynuclear images. Adding and adjusting the constraint parameter $\eta$ can effectively catch polynuclear contour in Figure 1. And the range of $\eta$ is $[2.5, 4]$ in our experiment for images in Figure 1.

The low contrast and multicellular images of 2018 Data Science Bowl can be segmented shown in Figure 3. The first column is input image, and we can find the difference which the second image in the first row is different from the first image. The reason is that using 1-D Legendre polynomials can effectually increase the contrast of image, like histogram equalization. Then, we get multicellular boundaries with ESF in equation (20).

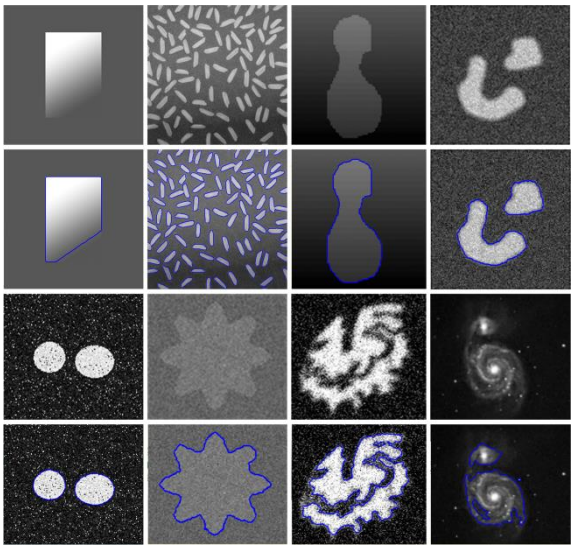

Figure 4: Segmentation results of our proposed method on synthetic and real images. (Blue curves are the final evolving curves.)

Similar to other existing methods, we conduct some experiments on synthetic and real images to prove greater generalization ability of our model in Figure 4. Large amounts of experiments show that our proposed model can take less time to converge and fewer iterations to converge. For example, the result of the first image in Figure 4 can be changed by adjusting $\eta$ and $g$ . If we set $m=0$ , $\eta=1$ and $g=0$ , it reduces to the SBGFRLS model. If we only set $\eta=1$ , the result is parallel to result of the LGLP model. Moreover, the proposed method can deal with noise images by adjusting $\sigma$ . The value of $\sigma$ is greater, and the final contour is more smooth.

To show the robustness of our model, we still make some experiments on colorized and multicellu -lar images in Figure 5. Especially for the second image in the first row, the size is $1000\times1000$ and our model can segment it faster than other models. In addition, we can see that the segmentation results of the second row is extremely accurate, comparing to ground truth in the third row. Note that the initial contour is set as multiple balls which are equally distributed with $r=30$ in the whole image.

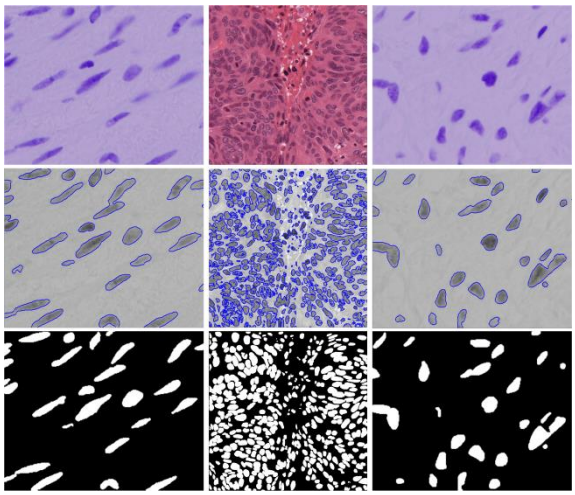

Figure 5: Segmentation results of our proposed method on colorized and multicellular images. Row 1: input images. Row 2: segmentation results. Row 3: ground truth. (The second image is one of the stage2_train data set, which is size of $1000\times1000$ .)

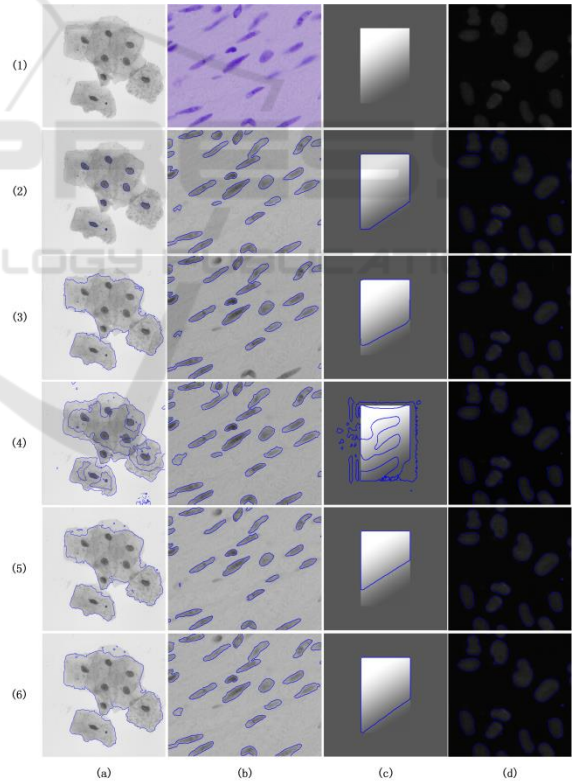


Figure 6: Comparison results on images with polynuclear, gray and multicellular, intensity inhomogeneity, and low-contrast multicellular. Row 1: input images. Row 2: results of the proposed method. Row 3: results of the L2S model. Row 4: results of the RSLGD model. Row5: results of the SBGFRLS model. Row 6: results of the LGLP model. (Blue curves are the final evolving curves.)

### 4.3 Performance Evaluation

From the above, the proposed model has three advantages, including the capability of catching multiple objects boundaries fast, dealing with noise and intensity inhomogeneity images effectively, and great generalization by adjusting $\eta$ . In the paper, we choose 4 different type models to make comparison in Figure 6. They are L2S, RSLGD, SBGFRLE, and LGLP respectively. As we see in Figure 6, images with polynuclear, gray and multicellular, intensity inhomogeneity, and low-contrast multicellular are chosen to support the above advantages. In a while, we utilize two quantitative analysis indexes, i.e. the iterations and required CPU time of segmentation results, to highlight the strengths of our model in Figure 7-8.

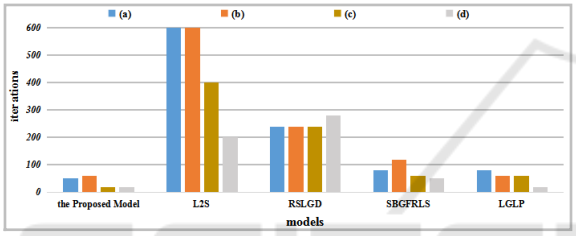


Figure 7: The iterations of different models in Figure 6. (From left to right: the proposed model, L2S, RSLGD, SBGFRLS, and LGLP.)

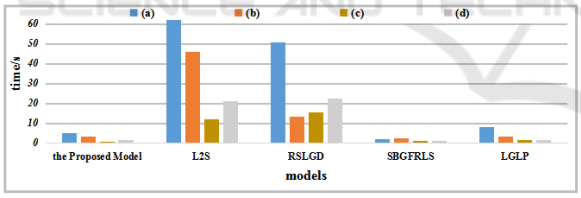


Figure 8: The CPU time of different models in Figure 6. (From left to right: the proposed model, L2S, RSLGD, SBGFRLS, and LGLP.)

In details, we still analyze the results of contrast experiments in Figure 6-8. The L2S model is one of region-based models. Even though we set a global initial level set function, we can't segment the whole objects like row 3. But 1-D Legendre polynomials in the model can efficaciously overcome intensity inho -mogeneity. Next, the RSLGD model can combine region and edge information by a new ESF to capture the object boundaries as far as possible. However, it has limitations that the gray value of image is Gaussian distribution like row 4 and col 3. A new region-based signed pressure force function is proposed in the SBGFRLE model, which can efficiently stop the contours at weak or blurred edges, but the model can't segment images with intensity inhomogeneity. Finally, the LGLP model combines L2S with SBGFRLE, and employs an ESF to capture the object boundaries fast. But it can't deal with polynuclear images.

Finally, the Figure 7-8 respectively explain the iterations and CPU time about the selected images in Figure 6. We can obtain that the proposed model is comparatively superior to other models.

## 5 CONCLUSIONS

In this paper, we has proposed a fast level set method which combines signed pressure force function with 1-D Legendre polynomial. To segment polynuclear images, we set a constrained parameter to adjust degree of convergence with regard to signed pressure force function. Besides, we set multiple ball contours for each image to reduce the costly re-initialization of the previous methods and possesses the characteristic of global segmentation. Meanwhile, we employ an ESF to capture the edge information and speed up the segmentation. Finally, compared with L2S, RSLGD, SBGFRLS and LGLP, our model not only enhances the ability of generali -zation, but also improves the efficiency and accura -cy of segmentation results for various nuclei images, especially for large size images.

## ACKNOWLEDGEMENTS

The work is supported by Ministry of The "ChunHui Plan" Fund Project of The Ministry of Education (Z2014085) and Chongqing Municipal Education Commission Project (KJ1601210) in College of Big Data and Intelligent Engineering, Yangtze Normal University.

## REFERENCES

Kass M, Witkin A, & Terzopoulos D. (1988). Snakes: Active contour models[J]. International Journal of Computer Vision, 1(4), 321-331.

Caselles V, Kimmel & R, Sapiro G. (1997). Geodesic active contours[J]. International Journal of Computer Vision, 22(1), 61-79.

Chan, T. F., & Vese, L. A. (2001). Active contours without edges[J]. IEEE Transactions on Image Processing, 10(2), 266-277.

Li, Chunming, Xu, Chenyang, Gui, Changfeng & Fox, M.D.. (2005). Level set evolution without re-initialization: A new variational formulation[C]. Proceedings of the IEEE Computer Society Conference on Computer Vision and Pattern Recognition. 1(1), 430- 436.

Li C L C , Kao C Y , & Gore J C , et al. (2007). Implicit Active Contours Driven by Local Binary Fitting Energy[C]. IEEE Conference on Computer Vision & Pattern Recognition, 1(1), 1-7.

Li C , Kao C Y , & Gore J C , et al. (2008). Minimization of Region-Scalable Fitting Energy for Image Segmentation[J]. IEEE Transactions on Image Processing, 17(10), 1940-1949.

Lankton S, & Tannenbaum A. (2008). Localizing Region-Based Active Contours[J]. IEEE Transactions on Image Processing, 17(11), 2029-2039.

Zhang K, Song H, & Zhang L. (2010). Active contours driven by local image fitting energy[J]. Pattern Recognition, 43(4), 1199-1206.

Li C , Xu C , & Gui C , et al. (2011). Distance Regularized Level Set Evolution and Its Application to Image Segmentation[J]. IEEE Transactions on Image Processing, 19(12), 3243-3254.

Zhang K , Zhang L , Song H , et al. (2010). Active contours with selective local or global segmentation: A new formulation and level set method[J]. Image and Vision Computing, 28(4), 668-676.

Wang X F, Huang D S, & Xu H. (2010). An efficient local Chan-Vese model for image segmentation[J]. Pattern Recognition, 43(3), 603-618.

Dai L , Ding J , & Yang J . (2015). Inhomogeneity-embedded active contour for natural image segmentation[J]. Pattern Recognition, 2015, 48(8), 2513-2529.

Abdelsamea, M. M. , & Tsaftaris, S. . (2013). Active contour model driven by globally signed region pressure force[C]. International Conference on Digital Signal Processing. IEEE.

Akram, F., Kim, J. H., & Choi, K. N.. (2013). Active Contour Method with Locally Computed Signed Pressure Force Function: An Application to Brain MR Image Segmentation[C]. Seventh International Conference on Image & Graphics. IEEE Computer Society, 1(1), 154-159.

Saini K , Dewal M L , & Rohit M. (2013). Level set based on new Signed Pressure Force Function for Echocardiographic image segmentation[J]. International Journal of Innovation & Applied Studies, 3(2), 560-569.

Wu Z, Gurari D, & Wong J Y , et al. (2012). Hierarchical Partial Matching and Segmentation of Interacting Cells[C]. International Conference on Medical Image Computing & Computer-assisted Intervention. Springer Berlin Heidelberg, 1(1), 389-396.

Park C , Huang J Z , & Ji J X , et al. (2013). Segmentation, Inference and Classification of Partially Overlapping Nanoparticles[J]. IEEE Transactions on Pattern Analysis and Machine Intelligence, 35(3), 1-1.

Mukherjee S, & Acton S T. (2014). Region Based Segmentation in Presence of Intensity Inhomogeneity Using Legendre Polynomials[J]. IEEE Signal Processing Letters, 22(3), 298-302.

Dai L, Ding J, & Yang J. (2015). Inhomogeneity-embedded active contour for natural image segmentation[J]. Pattern Recognition, 48(8), 2513-2529.

Sarkar R, Mukherjee S, & Acton S T. (2015). Dictionary Learning Level Set[J]. IEEE Signal Processing Letters, 22(11), 2034-2038.

Xing F, Xie Y, & Yang L. (2016). An Automatic Learning-Based Framework for Robust Nucleus Segmentation[J]. IEEE Transactions on Medical Imaging, 35(2), 550-566.

Zheng, S. , Fang, B. , Wang, P. S. P. , Li, L. , & Gao, M.. (2016). Multi-scale B-spline level set segmenta -tion based on Gaussian kernel equalization[C]. IEEE International Conference on Image Processing, 1(1), 4319-4323.

Zheng S , Fang B , & Li L , et al. (2017). Automatic Liver Lesion Segmentation in CT Combining Fully Convolutional Networks and Non-negative Matrix Factorization[J]. Imaging for Patient-Customized Simulations and Systems for Point-of-Care Ultrasound, 1(1), 44-51.

Zhang, Wei, Fang, Bin, Wu, Xuegang, Qian, Jiye, Yang, Weibin & Zheng, Shenhai. (2017). An improved active contour model driven by region-scalable and local Gaussian-distribution fitting energy[C]. International Conference on Security, Pattern Analysis, and Cybernetics, 1(1), 417-422.

Zhang, Kaihua, Zhang Lei, Lam Kin-Man, & Zhang David. (2016). A Level Set Approach to Image Segmentation With Intensity Inhomogeneity. 1(1), 546-557.

Chen G , Chen M , & Li J , et al. (2017). Retina Image Vessel Segmentation Using a Hybrid CGLI Level Set Method[J]. Biomed Research International, 1(1), 1-11.

Lee C H , Soomro S , & Akram F , et al. (2017). Segmentation of Left and Right Ventricles in Cardiac MRI Using Active Contours[J]. Computational and Mathematical Methods in Medicine, 1(1), 1-16.

Min H , Jia W , & Zhao Y , et al. (2018). LATE: A Level-Set Method Based on Local Approximation of Taylor Expansion for Segmenting Intensity Inhomogeneous Images[J]. IEEE Transactions on Image Processing A Publication of the IEEE Signal Processing Society, 27(10), 5016-5.31.

He, Guanghui, Yang, Guangfang, Fang, Bin & Zhang, Wei. (2018). An Improved Local or Global Active Contour Driven by Legendre Polynomials[C]. International Conference on Wavelet Analysis and Pattern Recognition, 1(1), 23-28.